scientific reports

OPEN

Fast singlet excited-state deactivation pathway of flavin with a trimethoxyphenyl derivative

Stanisław Niziński[1,2], Naisargi Varma[3], Marek Sikorski[3 ✉], Tomáš Tobrman[4], Eva Svobodová[4], Radek Cibulka[4 ✉], Michał F. Rode[5 ✉] & Gotard Burdzinski[2 ✉]

Incorporation of the trimethoxyphenyl group at position 7 of flavin can drastically change the photophysical properties of flavin. We show unique fast singlet $^1(\pi,\pi^*)$ excited state deactivation pathway through nonadiabatic transition to the $^1(n,\pi^*)$ excited- state, and subsequent deactivation to the ground electronic state (S_0), closing the photocycle. This mechanism explains the exceptionally weak fluorescence and the short excited–state lifetime for the flavin trimethoxyphenyl derivative and the lack of excited triplet T_1 state formation. Full recovery of flavin in its ground state takes place within a 15 ps time window after photoexcitation in a polar solvent such as acetonitrile. According to quantum chemical calculations, the $C_{(2)}$-O distance elongates by 0.16 Å in the $^1(n,\pi^*)$ state, with respect to the ground state. Intermediate–state structures are predicted by theoretical ab initio calculations and their dynamics are investigated using broadband vis-NIR time-resolved transient absorption and fluorescence up-conversion techniques.

Keywords Flavin, Isoalloxazine, Photophysics, Excited state ab initio calculations, Time-resolved spectroscopy

Flavins are important biologically active molecules with a structure characterized by isoalloxazine core (see Fig. 1)[1,2]. Flavin cofactors, such as flavin mononucleotide (FMN) and flavin adenine dinucleotide (FAD), which are derived from riboflavin (Fig. 1), are mainly involved in dark enzymatic redox reactions. Nevertheless, the role of flavins in light-dependent processes[3] such as bioluminescence, plant phototropism, nucleic acid repair, and the regulation of biological clocks, has been documented and is currently the subject of intensive research. Artificial flavin derivatives are also important compounds used in organocatalysis and in organic photoredox catalysis[2,4–8].

Photophysics of flavin (**Fl**) derivatives is rich and well-studied[9–14]. Their photoexcitation leads to the population of the $^1(\pi,\pi^*)$ singlet excited state (S_1), which typically relaxes through $S_1(\pi,\pi^*) \to S_0$ radiative decay and $S_1 \to T_1$ intersystem crossing. In aerobic solutions, the nascent T_1 species sensitizes singlet oxygen ($^1O_2$) with a yield close to the **Fl** triplet formation quantum yield Φ_{T1}. For example, 3,10-dimethylisoalloxazine **4** (Fig. 1) in acetonitrile is characterized by a high yield of singlet oxygen sensitization, $\Phi_\Delta = 0.56$[15]. Moreover, its singlet excited-state lifetime τ_{S1} is long (7.0 ns)[16]. To suppress triplet state formation and fluorescence, a very fast competing deactivation channel of the S_1 state is required.

Flavins are studied not only experimentally but also theoretically. A variety of quantum chemical methods have been applied to the study of flavins in their different oxidized and reduced forms. For a detailed discussion, readers are referred to an excellent review that describes several methods: starting from DFT gas-phase approaches and the simple polarizable continuum model, through the QM-cluster model, the fragment molecular orbital (FMO) method featuring molecular orbitals of fragments, the hybrid quantum mechanics molecular mechanics QM/MM method, the extrapolative scheme known as ONIOM (short for 'Our own N-layered Integrated molecular Orbital and Molecular mechanics'), and up to the scheme of QM/MM calculations where the MM atoms are replaced with their partial (point) charges[17]. Particularly noteworthy are the papers in which the electronic structure of flavin has been discussed in a context of position and character of substituents[14,18–20] and effect of environment[21,22]. In recent contribution a variety of electronic structure methods were studied to

[1]Department of Biomolecular Mechanisms, Max Planck Institute for Medical Research, Jahnstrasse 29, 69120 Heidelberg, Germany. [2]Faculty of Physics and Astronomy, Adam Mickiewicz University, Uniwersytetu Poznanskiego 2, 61-614 Poznan, Poland. [3]Faculty of Chemistry, Adam Mickiewicz University, Uniwersytetu Poznanskiego 8, 61-614 Poznan, Poland. [4]Department of Organic Chemistry, University of Chemistry and Technology, Prague, 16628 Prague, Czech Republic. [5]Institute of Physics, Polish Academy of Sciences, Aleja Lotników 32/46, 02-668 Warsaw, Poland. ✉email: sikorski@amu.edu.pl; radek.cibulka@vscht.cz; mrode@ifpan.edu.pl; gotardb@amu.edu.pl

describe the energetics of the low-lying excited states $^1(\pi,\pi^*)$ and $^1(n,\pi^*)$ of flavin, including the potential-energy scans tracing the coordinates form the Franck-Condon point to $^1(\pi,\pi^*)$ minimum and then towards $^1(n,\pi^*)$ minimum[23].

Tuning the spectral and electronic properties of **Fl** is required for applications in **Fl**-mediated organocatalytic and photocatalytic reactions[2,4,7,8,24–26]. So far, it is believed that fully oxidized flavins exhibit good fluorescence quantum yield, usually accompanied by high triplet quantum yield and the associated efficiency of singlet oxygen formation. Extreme cases are e.g. reduced flavins which are essentially nonfluorescent, having a quantum yield more than three orders of magnitude lower than oxidized flavins[27]. As an example of typical flavin photophysics, compound **4** (Fig. 1) can be given, which has high fluorescence quantum yield ($\Phi_f = 0.35$) and long $^1(\pi,\pi^*)$ state lifetime (7 ns) in acetonitrile[15,16]. Recent synthetic efforts have demonstrated effective methods for synthesis of **Fl** derivatives by installing aryl substituents at the position 7 via direct C−C bonding[15]. To our surprise, along newly synthesized flavin derivative **1** with trimethoxyphenyl group at the position 7 (Fig. 1), exhibits a very weak fluorescence which is unique among flavin derivatives. Thus, this work is devoted to elucidating the mechanism of enhancement in radiationless relaxation of the singlet excited state in the flavin substituted by 3,4,5-trimethoxyphenyl group in the position 7. Complementary experimental and theoretical studies show that incorporation of trimethoxyphenyl group into isoalloxazine activates a fast $^1(\pi,\pi^*) \rightarrow {}^1(n,\pi^*) \rightarrow S_0$ nonradiative channel. This finding is expected to hold for flavins in general and can be used to tune their photophysics, when fast light-to-heat conversion is desired, without formation of the reactive species such as singlet oxygen, $^1O_2$.

Experimental
Materials
The investigated flavin derivative, 7-(3,4,5-trimethoxyphenyl)isoalloxazine **1** (see Fig. 1), was prepared by Suzuki coupling starting from the corresponding 7-bromoisoalloxazine derivative[15]. The reference compound 3,10-dimethylisoalloxazine **4** was prepared according to literature[28].
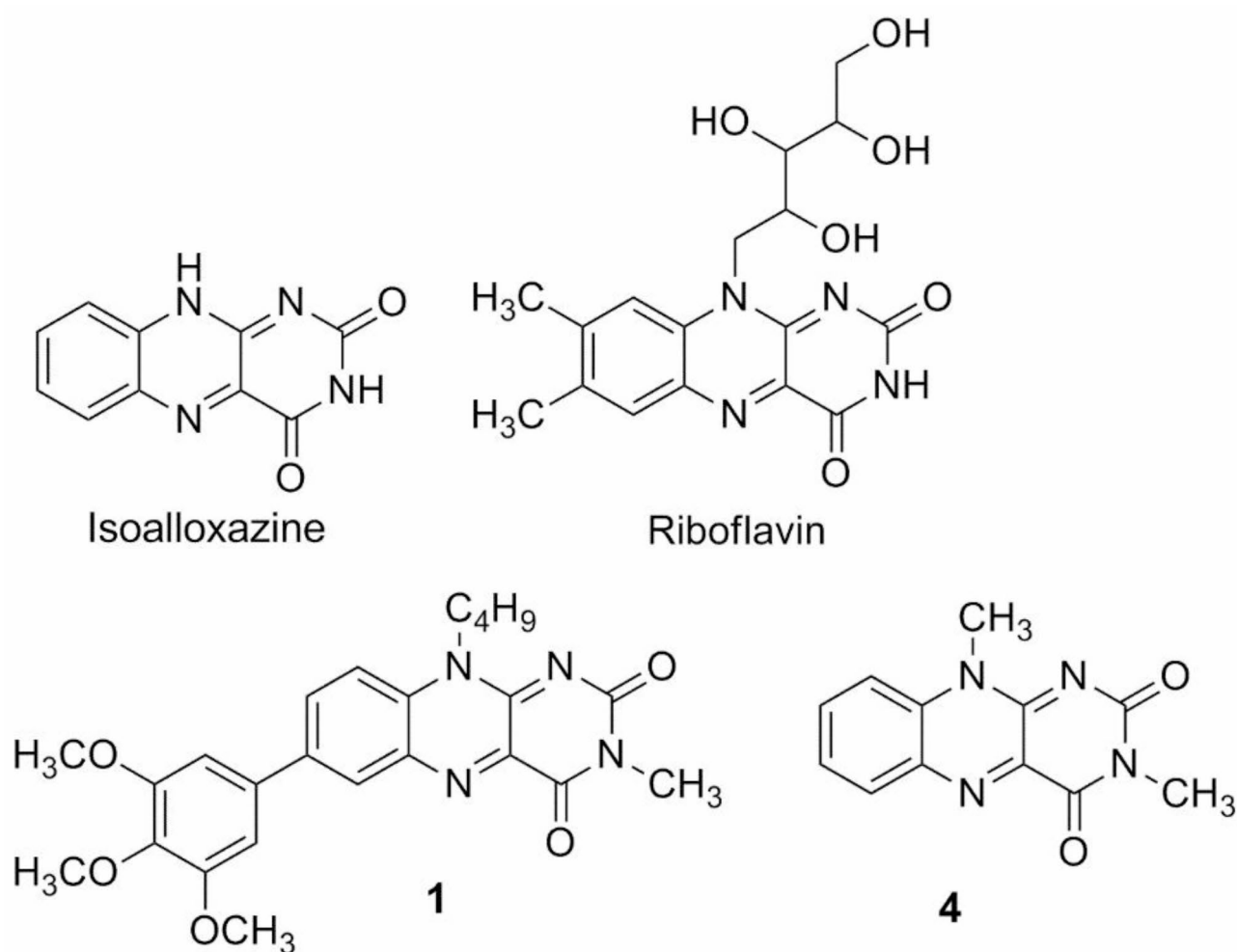

Fig. 1. Structure of isoalloxazine as the parent structure of flavins, riboflavin as an example of naturally occurring flavins, and flavins **1** and **4** which are subject to investigation in this work.

Stationary fluorescence

Fluorescence emission spectra were recorded on a Horiba Jobin- Yvon-Spex Fluorolog 3–22 spectrofluorometer[29]. Right-angle geometry was used in all of the steady-state emission measurements. The experiments were performed on 3.5 mL of sample solutions contained in a quartz cell (1 cm × 1 cm) using the linear fit method. Fluorescence spectra were collected with 3 nm excitation and 3 nm emission slits, using 0.1 s integration time. Lumichrome in acetonitrile with 0.028 fluorescence quantum yield (Φ_f) was used as a reference standard[11].

Femtosecond fluorescence up-conversion

Femtosecond fluorescence up-conversion measurements (Figure S1) were performed in a 2 mm thick quartz cell. Sample solution was stirred by a Teflon-coated bar. The sample of **1** was prepared in acetonitrile with absorbance A(2 mm) = 0.2 at the excitation wavelength 400 nm. The details of the experimental set-up is given in Supporting Information file. The molecular rotational diffusion effects were eliminated by using a magic-angle configuration. Fitting of the fluorescence kinetic was performed with a single-exponential function convoluted with Gaussian IRF using lmfit library in Python[30] optimization algorithm applied was Levenberg-Marquardt. Obtained FWHM of the IRF was 400 fs.

Femtosecond UV–Vis–NIR transient absorption

Femtosecond UV–vis-NIR transient absorption spectra were obtained using a commercially available system (Ultrafast Systems, Helios)[31,32]. The solution of **1** were studied in a 2 mm thick quartz cell with a steering magnetic bar. Experiments were performed at the excitation wavelength of 500 nm, with 1 µJ energy per pulse (photon peak fluence $\approx 2 \times 10^{15}$ photons per cm²). The pump diameter (FWHM) at the sample was ≈250 µm. Probing white light continuum pulse was generated in a sapphire plate (visible range) or in YAG crystal (NIR range). The recorded transient absorption spectra were corrected for the chirp using Surface Xplorer software. The kinetics were analyzed using fitting procedure (Surface Xplorer), satisfactory fits were typically obtained with two-exponential function. Convolution with the instrument response function (ca. 200 fs FWHM) was included into the fitting procedure.

Computational details

The photophysics of flavin derivatives **1–4** (see Fig. 6) were studied separately by means of ab initio methods both in the ground (S_0) and excited (S_1) electronic states. Each of molecules **2–4** have a single distinguished minimum in the ground electronic state (S_0). The molecule **1** has two close-in energy minima with the hydrogen-bonded minimum (H-bonded, Table 2) slightly lower, and this latter minimum has the reference energy of the whole system. The geometries in their closed-shell ground electronic state, S_0, were determined with the MP2 method[33] without symmetry constraint and the MP2 energy of this form (in the S_0-state) is the reference value for all other ground-state and excited-state structures. The excited-state (S_1) equilibrium geometries were determined with the second-order algebraic diagrammatic construction ADC(2) method[34–37]. Each molecule has three equilibrium excited-state geometries: $S_1^{LE}(\pi,\pi^\star)$, $S_1^{LD}(n,\pi^\star)$ and $S_1^{LU}(n,\pi^\star)$ and each of them was optimized without any symmetry constraints. In terms of the geometry, the most apparent difference between them lies in the length of the optimized $C_{(2)}$-O and $C_{(4)}$-O bond lengths (see Table 3) which make them coordinates for the S_1-state deactivation mechanism. All four geometries: one ground state and three excited states differ also with the interatomic distances of the carbon-carbon skeleton inside the flavin rings – especially one ring possessing carbonyl groups (see Table S1).

To find fast singlet excited-state deactivation paths of **1**, the three excited states were determined: one $\pi\pi^\star$ excited state, $S_1(\pi,\pi^\star)$, and two $(n,\pi^\star)$ excited states characterized by a substantial elongation of one of the two carbonyl bonds present in the molecules (marked LD and LU). To study this process, the relaxed potential-energy profiles were constructed, separately in the S_0 and the excited states: $S_1^{LE}(\pi,\pi^\star)$, $S_1^{LD}(n,\pi^\star)$ and $S_1^{LU}(n,\pi^\star)$, along the $R_1(C_{(2)}$-O) distance driving coordinate. For each fixed value of a given $R_1(C_{(2)}$-O) coordinate the remaining 3N-7 internal nuclear coordinates were optimized. In this way each of the excited-state minimum of the given molecule is depicted in the excited-state potential-energy profile with its characteristic $R_1(C_{(2)}$-O) distance (see Fig. S3).

For each molecule, the correlation-consistent valence double-zeta basis set with polarization functions on all atoms (cc-pVDZ)[38] was used in these calculations as well as in the calculations of the potential-energy profiles.

To simulate the UV absorption spectra, the simplified version of the coupled clusters method was used, CC2[39,40] in conjunction with the aug-cc-pVDZ[38] basis set. All the calculations were performed using the TURBOMOLE program package[41].

Experimental results

UV–Vis absorption spectra and weak fluorescence

Compound **1** in acetonitrile shows an absorption band with a long wavelength maximum at 462 nm (2.69 eV) corresponding to $\pi \rightarrow \pi^\star$ transition (Fig. 2A). The determined extinction coefficient is ε(462 nm) = 8560 M⁻¹ cm⁻¹. This absorption band is consistent with the CC2/aug-cc-pVDZ calculated value for $\Delta E^{VE}(S_0 \rightarrow S_1(\pi\pi^\star))$ of 2.76 eV for weakly H-bonded isomer and of 2.89 eV for just by 0.026 eV less stable non-hydrogen bonded isomer of **1** (see Table 2). The fluorescence spectrum recorded upon excitation at 463 nm shows an $S_1 \rightarrow S_0$ fluorescence band with maximum at 528 nm (2.35 eV) (Fig. 2B). The calculated fluorescence energy value from the relaxed emitting $S_1(\pi\pi^\star)$ state minima, E_{fl}, equals 1.93 eV (ADC(2)/cc-pVDZ) – for non-H-bonded rotamer, and 1.70 eV – for H-bonded excited state (see Table 3). Single point calculations at the CC2/aug-cc-pVDZ level for those two emitting forms give E_{fl} values more close to experimental 2.35 eV value: 2.09 (non-H-bonded) and 1.90 eV (H-bonded), respectively. The experimentally determined fluorescence quantum yield is very low of $\Phi_f = 2.6 \times 10^{-4}$ in acetonitrile, probably implying a very short $\tau_{S1}(\pi,\pi^\star)$ lifetime.
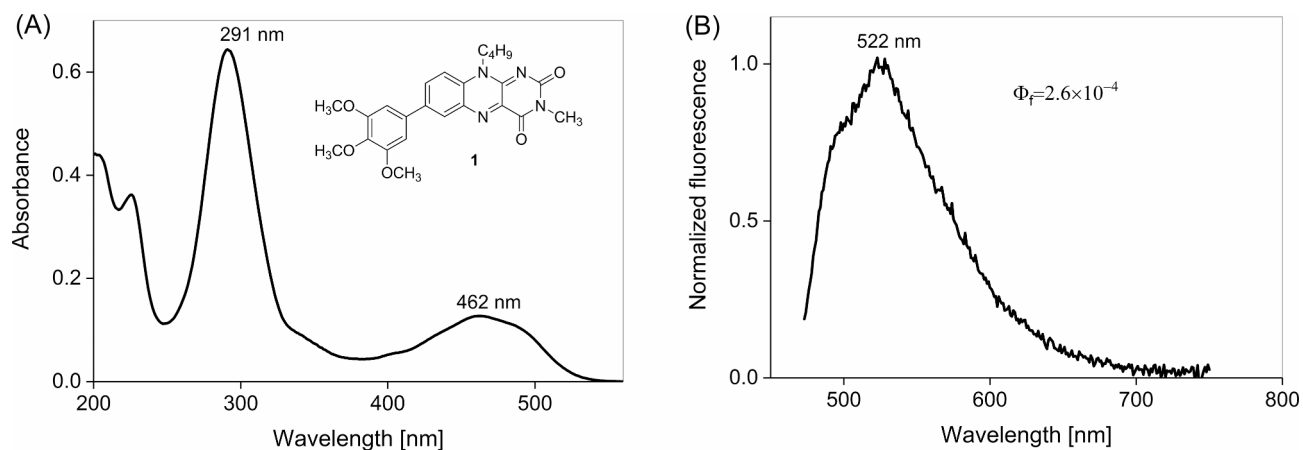
Fig. 2. (**A**) Stationary UV-Vis absorption spectrum and (**B**) fluorescence spectrum of **1** in acetonitrile ($\lambda_{exc} = 463$ nm).

Emission kinetics recorded with fluorescence up-conversion spectroscopy

Excitation of compound **1** in acetonitrile at 400 nm results in kinetics showing a surprisingly fast $S_1(\pi,\pi^*) \rightarrow S_0$ fluorescence decay. A single-exponential fit of kinetics shown in Fig. 3, indicates a very short $\tau_{S_1}(\pi,\pi^*)$ lifetime of 0.41 ps, about 3 orders of magnitude shorter than typical τ_{S_1} lifetimes reported for **Fls**, including reference **4** (Table S2)[9]. This surprising property is caused by the presence of the trimethoxyphenyl group in compound **1**. To get further insights into mechanism of $S_1(\pi,\pi^*)$ deactivation, transient absorption studies were performed.

Transient species in NIR spectral range

For transient absorption measurements of **1** in NIR spectral range, 500 nm (2.5 eV) excitation wavelength λ_{ex} has been selected in order to populate $S_1(\pi,\pi^*)$ state without significant excess of vibrational energy. This λ_{ex} lies little further in red than λ^{max} absorption band peak (Fig. 2). The transient absorption experiment reveals an instantaneous formation of the band centered about 1500 nm which can be assigned to the $S_1(\pi,\pi^*)$ state absorption ($S_1 \rightarrow S_n$ transition, Fig. 4A). This band decays with a time-constant of ca. 470 fs which is the lifetime of the $S_1(\pi,\pi^*)$ state (Fig. 4B), in a good agreement with fluorescence up-conversion spectroscopy data (0.41 ps). Subsequently, we observed the appearance of the band at about 1000 nm (Fig. 4C), which can tentatively be assigned to the $^1(n,\pi^*)$ state population as its rise (ca. 430 fs) matches the decay time-constant of the precursor $-^1(\pi,\pi^*)$ state. The $^1(n,\pi^*)$ population undergoes decay over time-scale of a few picoseconds, described by the time-constant $\tau_{S_1}(n,\pi^*)$ of 2.1 ps. In contrast to the NIR range, recorded transient absorption spectra in the visible spectral range show a higher complexity due to the contribution of the S_0 ground state bleaching and $S_1(\pi,\pi^*) \rightarrow S_0$ stimulated emission.

Transient species in the visible range

The transient absorption kinetics at 650 nm (Fig. 5B) reveal a rapidly-decaying negative signal corresponding to $S_1(\pi,\pi^*) \rightarrow S_0$ stimulated emission associated with a time constant of 0.62 ps. Disappearance of that signal is followed by a rise of the positive transient absorption signal, reaching maximum at a delay time of 1.5 ps. It can be assigned to $^1(n,\pi^*)$ population. The presence of a short-lived (0.66 ps, Fig. 5C) positive signal at 473 nm can also be attributed to the $S_1(\pi,\pi^*)$ population. The contour plot of the transient absorption data (Fig. 5A) gathers these signals together, illustrating the interplay between them.

The kinetics probed at 541 nm is dominated by the absorption of $S_1(n,\pi^*)$ population (Fig. 5D). The decay occurs with a relatively long 3 ps time constant (not approximately 2.2 ps, as probed at 650 and 1015 nm, Table 1). This may be a manifestation of the additional contribution from the hot S_0 ground state population nascent upon $^1(n,\pi^*)$ state decay. The nascent hot S_0 state may undergo absorption band narrowing upon shedding its excess heat to the solvent[31]. Indeed, inspection of the kinetics probed at 473 nm (Fig. 5C) shows that repopulation of the ground state S_0 occurs with a relatively long time constant of 3.4 ps, suggesting that S_0 vibrational cooling of compound **1** is likely the rate limiting step. Note that the complete recovery of the S_0 population observed within a 15 ps time window (Fig. 5A), indicates the return of molecules of compound **1** to their initial form, as existed before sample photoexcitation, and no longlived intermediates (such as triplet species) remain. This photobehavior of compound **1** is dramatically different from typical **Fl** photophysics, which are known for active triplet generation in the intersystem crossing $T_1 \leftarrow S_1$[9,11]. For instance, the reference compound **4** after photoexcitation at 470 nm shows a gentle decay of the population of the S_1 state in a temporal window of 2.6 ns and the appearance of the absorption band of the T_1 state (Fig. S2A), similar characteristics have been reported for deazaflavin (3-butyl-10-methyl-5-deazaisoalloxazine)[42].
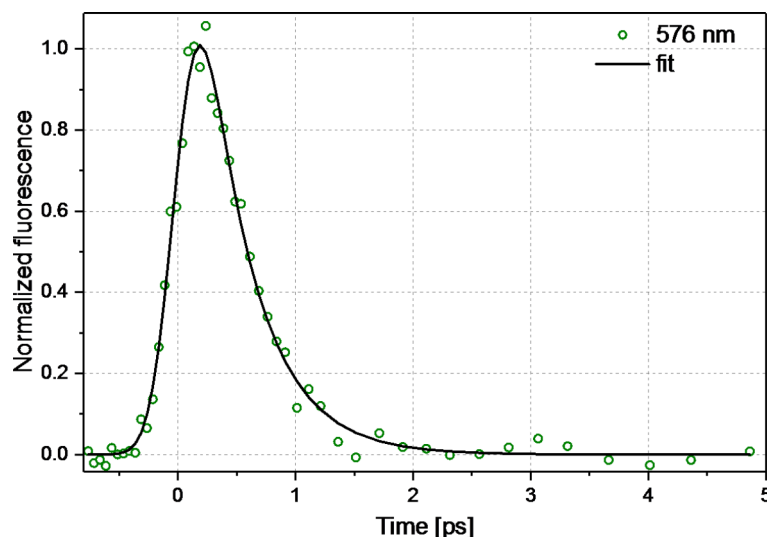
Fig. 3. Kinetics of fluorescence of **1** (c = 3.0 × 10⁻⁴ M) in acetonitrile probed at 576 nm after excitation at 400 nm (0.25 μJ). The single exponential fit convoled with Gaussian with IRF = 400 fs, resulted in τ = 0.41 ps.

Comparison of the simulated UV–Vis absorption spectra and S₀-state geometry of molecule 1 with other Fl derivatives

The experimentally studied molecule **1** consists of the two moieties: an almost planar 3-methylisoalloxazine ring covalently bound to a trimethoxyphenyl group attached at the position 7. The presence of the additional butyl group – attached to the nitrogen atom $N_{(10)}$ – is the reason for existence of two low-energy rotamers (Table 2). The most stable one is a weakly hydrogen bonded rotamer in which the butyl group interacts with the $N_{(1)}$ atom with the intramolecular hydrogen bond distance $C_{(4')}H—N_{(1)}$ is of 2.49 Å. The second-in-energy rotamer – in which the butyl group is tilted away from the flavin moiety– molecule is by 0.026 eV less stable (MP2/cc-pVDZ). The small energy difference between them make it possible that both rotamers coexist in thermal equilibrium, in experimental conditions - especially in polar solvent which should stabilize more polar non-H-bonded isomer (7D vs. 6.5D). To understand better a fast deactivation of the S₁ excited-state of molecule **1**, three other molecules, **2**, **3** and **4** were selected for calculations (Fig. 6). While the molecule **4** consists of just unsubstituted isoalloxazine skeleton, the remaining two, **2** ad **3**, have an additional substituent – attached to the position 7 of flavin – with increasing electron donating character: phenyl (molecule **3**) and trimethoxyphenyl (molecule **2**). Note that in derivatives **2–4**, the butyl substituent is replaced by the methyl group to study sole electronic effect of the step-by step substitution of the molecule **4**. Moreover, **4** is an excellent reference (Fig. S2B), since its slow S₁-state deactivation (τ_{s1} = 7 ns in acetonitrile) has been reported[16].

The calculations were aimed to determine the geometry of the **Fl** derivatives in the electronic ground state S₀ and the excited states S₁(π,π*) and S₁(n,π*). Interestingly, the distances $R_1(C_{(2)}-O)$ and $R_2(C_{(4)}-O)$ were found to be substantially different in these states (Fig. 6).

Calculations show that for molecule **1** the twist angle (C-C-C-C dihedral) of the trimethoxyphenyl vs. isoalloxazine ring is approximately 39° in the minimum ground-state S₀, while both carbonyl bonds $R_1(C_{(2)}-O)$ and $R_2(C_{(4)}-O)$ are short, having length of 1.222 and 1.223 Å, respectively (see Table 3). Those geometrical parameters of **1** are very comparable to the derivatives: **2** and **3** (see Fig. 6) while the R_1 and R_2 distances also to **4**. The calculated vertical excitation energies, ΔE^{VE}, to the lowest singlet excited states for molecules **1–4** are gathered in Table 2. According to these calculations, the S₀ → S₁ transition energy for H-bonded isomer of **1**, $\Delta E^{VE}(S_0{\rightarrow}S_1)$ of 2.76 eV (λ_{abs} = 450 nm, CC2/aug-cc-pVDZ), has a substantial oscillator strength, f of 0.2, which is the highest f value among all the S₀ → Sₙ transitions (up to n = 6). The S₀ → S₁(π,π*) transition is also the strongest for the remaining molecules studied: **2–4**. What varies is the value of $\Delta E^{VE}(S_0 \rightarrow S_1(π,π^*))$ which decreases in the series from 3.01 eV, for unsubstituted **4**, through 2.83 eV, for phenyl-substituted **3**, and 2.77 eV, for 7-trimethoxyphenylisoalloxazine **2** down to 2.76 eV for **1**. In comparison to unsubstituted molecule **4**, the presence of phenyl, in **3**, and three methoxyphenyl groups, in **1** and **2**, decreases the ΔE^{VE} value for the S₀ → S₁(π,π*) transition leaving the S₀ → Sₙ(n,π*) transitions almost unchanged. Both groups are strong π-electron donors[43,44] and they tend to stabilize the ¹π,π* excited states. Thus they lower either the vertical excitation energies, $\Delta E^{VE}(S_0{\rightarrow}π,π^*)$, or adiabatic energies, E^a, of the optimized (¹π,π*) excited state (see Tables 2 and 3). Similar substituent effect has been reported[45]. As it is shown in Table S3, the presence of the π-electron donating methoxy group results in a shift of the electron density from the π occupied orbital localized on the trimethoxyphenyl to the π* unoccupied orbital localized solely on the flavin.

Table 3 shows that the state S₁(π,π*) has substantially high dipole moment μ_e, thus one can expect that the use of polar solvent can further stabilize this state.
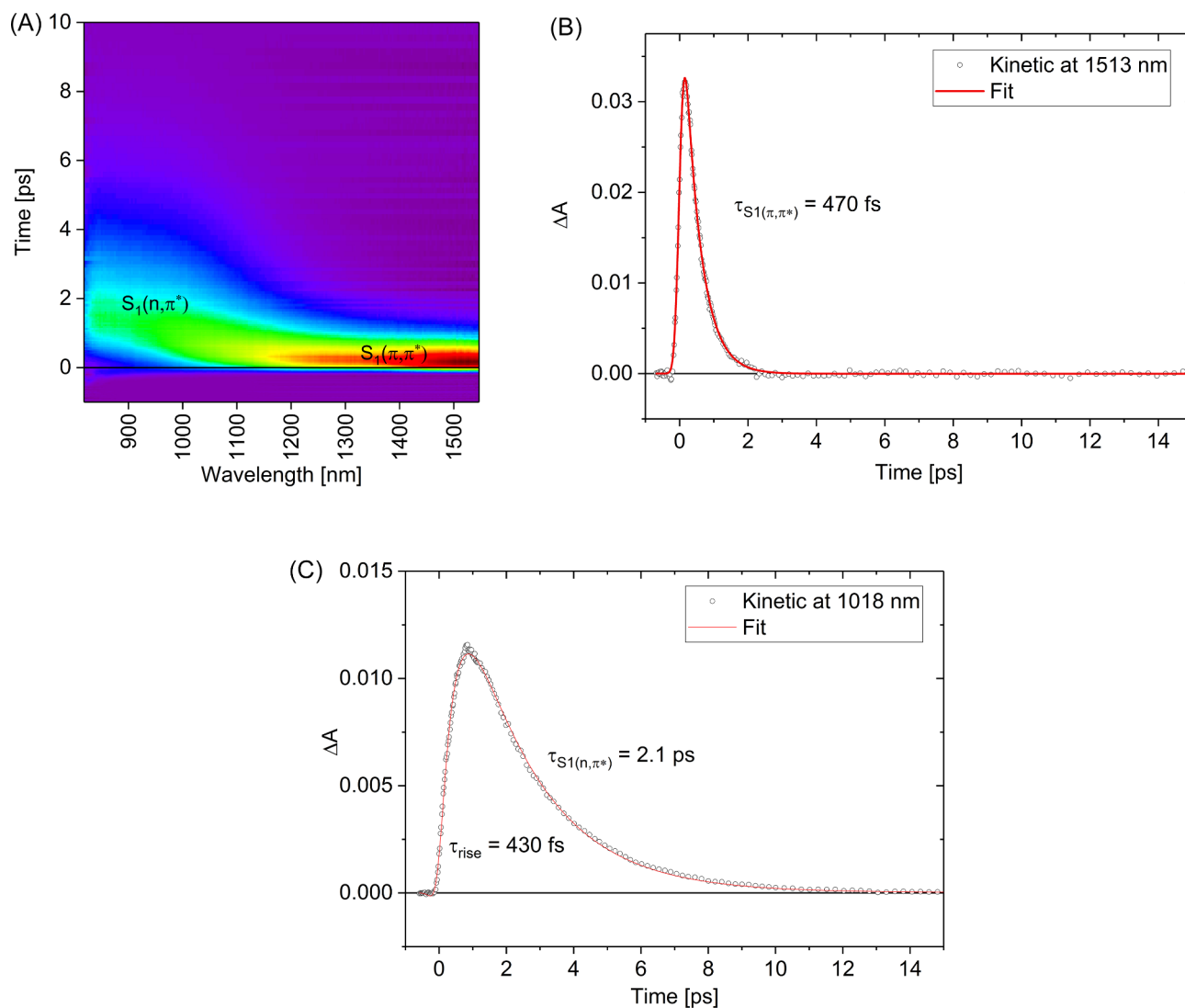
Fig. 4. Transient absorption data in NIR spectral range for **1** ($c = 3.9 \times 10^{-4}$ M) in acetonitrile upon excitation at 500 nm (1 µJ). Contour plot (**A**) and selected representative kinetics at 1513 nm (**B**) and 1018 nm (**C**).

The mechanism of the singlet excited-state deactivation

The S_0 ground state energy landscape of the molecule **1** consists of two close-in-energy minima related to H-bonded and non-H-bonded isomers (see Table 2), while the derivatives **2–4** have a single global minimum. All the minima have short C=O double bonds – with an increasing potential-energy when elongating one of the carbonyl bonds (see black filled circles in Fig. 7). The excited-state energy landscape is much more diverse and chemical structure dependent.

The electronic structure of molecule **1** is determined mainly by its ground S_0 state and three singlet excited–state forms: one $^1\pi\pi^*$ and two $^1n\pi^*$ states. These excited–state equilibrium geometries, optimized without any symmetry constraint, differ mainly in terms of carbonyl bond elongation and by the C-C and C-N bond distances in their close vicinity, as in thymine[46]. The twisting angle of the trimethoxyphenyl moiety vs. flavin is close to 40º for those excited-state forms.

Each of the $^1n\pi^*$ state minima is characterized by the elongation of one of the C-O carbonyl bonds present in flavin moiety (as shown in Fig. 6). Each C-O elongation is related to the excitation of an electron from the orbital "n" lone pair of the given oxygen atom – localized on this C-O bond – to the antibonding orbital π^* delocalized throughout the molecule. The described excitation can be traced in Table S3, where it is shown that both n and π^* orbitals are localized on flavin which means that both the $S_1(n,\pi^*)$ states are the local states also of unsubstituted flavin. What is different for the $S_1^{LE}(\pi,\pi^*)$ excited state minimum is that the electron is photoexcited from the occupied π orbital localized also on trimethoxyphenyl substituent to the π^* orbital localized exclusively on the flavin. This way, the π-electron donating character of the methoxy groups is seen as it pushes the electron density from phenyl towards flavin, in the $S_1^{LE}(\pi,\pi^*)$ state, favoring its stabilization vs. the $S_1(n,\pi^*)$ states.

We distinguish two: $S_1^{LD}(n,\pi^*)$ and $S_1^{LU}(n,\pi^*)$ singlet $^1n\pi^*$ excited states, each associated with the elongation of a different C-O bond. At the $S_1^{LD}(n,\pi^*)$ minimum, the $C_{(4)}$-O bond is much longer than the $C_{(2)}$-O bond

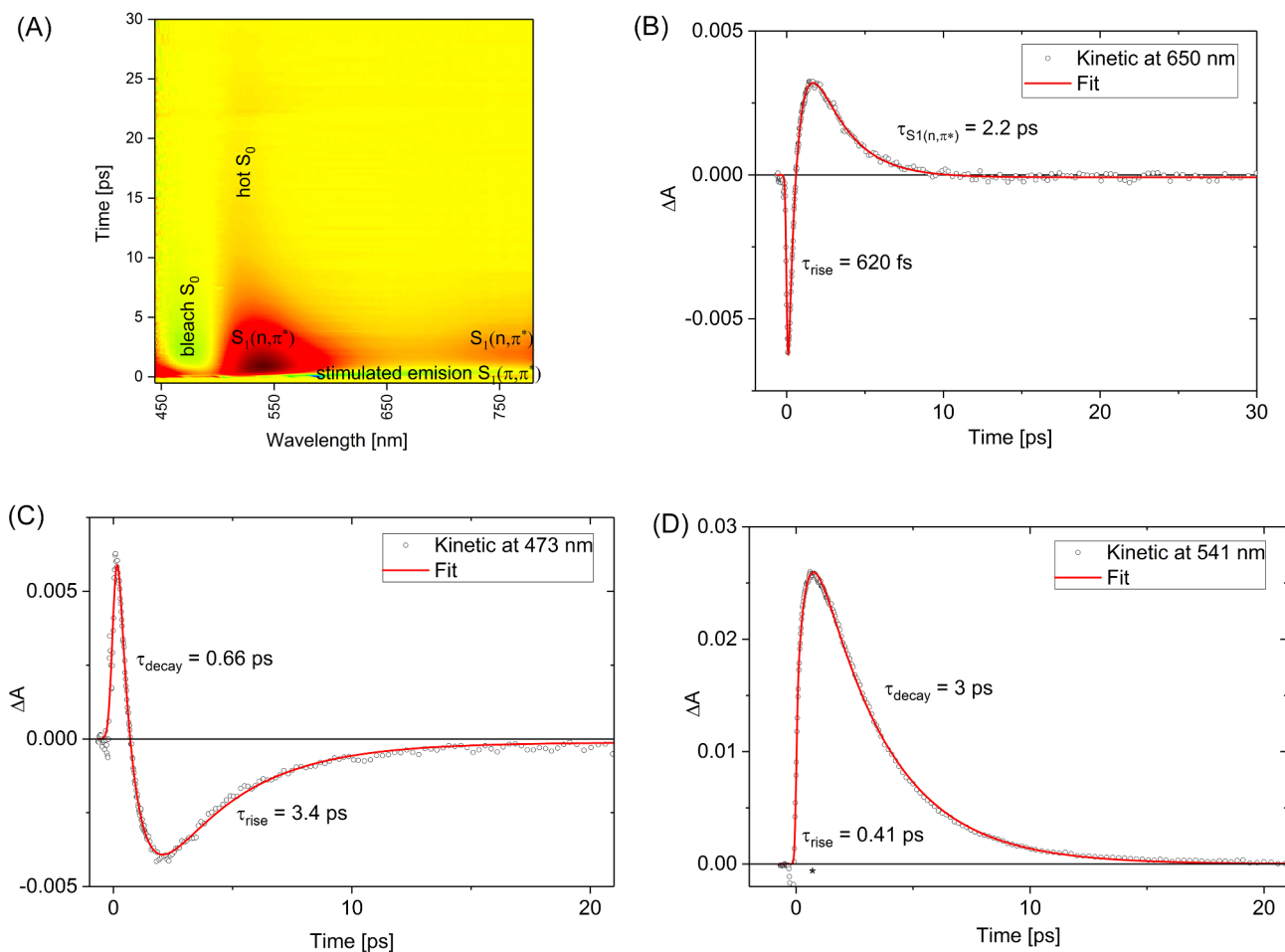**Fig. 5**. Transient absorption data recorded in visible range for **1** (c = 3.9 × 10⁻⁴ M) in acetonitrile upon excitation at 500 nm (1 μJ). Contour plot (**A**) and selected representative kinetics at 650 nm (**B**), 473 nm (**C**) and 541 nm (**D**). (*) solvent contribution.

($R_2 > R_1$) while the proximal $C_{(4)}$-C and $C_{(4)}$-$N_{(3)}$ bonds are shorter than in the S_0-state geometry. In the case of the $S_1^{LU}(n,\pi^*)$ minimum, the C_2-O bond is much longer ($R_2 < R_1$) and the $C_{(2)}$-$N_{(1)}$ and $C_{(2)}$-$N_{(3)}$ bonds get substantially shrinked. To trace the excited–state decay mechanism, we will examine molecule **1** through computational studies and compare it with the profiles obtained for unsubstituted derivative **4** (molecules **2** and **3** are provided in Figure S3).

Upon photon absorption, the first locally excited state $S_1^{LE}(\pi,\pi^*)$ is populated as the $S_0 \rightarrow S_1$ transition is characterized by a high oscillator strength (Table 2). Initially, the system relaxes to the equilibrium form of this $S_1^{LE}(\pi,\pi^*)$ state, as its geometry closely resembles the geometry of the S_0-state, especially in terms of two short C-O bonds (see the blue curve Fig. 7A, for molecule **1**, and Fig. 7B, for molecule **4**). The $S_1^{LE}(\pi,\pi^*)$ state is predicted to be a fluorescent state, with the fluorescence energy, E_{fl}, for molecule **1** being 1.90 eV ($\lambda_{fl}^{calc} = 653$ nm) for H-bonded isomer obtained by single-point CC2/aug-cc-pVDZ. However, the profile of the $S_1^{LE}(\pi,\pi^*)$ state is very shallow (see blue filled squares along the solid line in Fig. 7A) with a tiny excited-state barrier of 0.001 eV (at $R_1 = 1.255$ Å). Behind the barrier, only two additional points were optimized in this state with slightly lower energy (up to $R_1 = 1.258$ Å) and further attempts in optimization of the first singlet state at little larger distances produced the molecule in the $S_1^{LU}(n,\pi^*)$ state. This is an indication that the molecule finds the CI region between the two excited states. We tried, however, to find more evidence of such a situation, and additional calculations were performed. (i) Optimization of the second excited state was performed at the few distances $R_1 > 1.258$ Å and those calculations ended up in finding two almost degenerate states: $S_1^{LE}(\pi,\pi^*)$ and $S_1^{LU}(n,\pi^*)$ suggesting existence of the crossing point. (ii) Second, the single-point calculations of the few lowest excited states were performed on top of the profiles of the $S_1^{LE}(\pi,\pi^*)$ and $S_1(n,\pi^*)$ exited states (LU and LD, Fig. S4). The $S_1^{LE}(\pi,\pi^*)$ state calculated with the geometry of the $S_1^{LU}(n,\pi^*)$ state for molecule **1** is quite close in energy to the lower $S_1^{LU}(n,\pi^*)$ state indicating the proximity of the region CI($^1\pi\pi^*/^1n\pi^*$), at a distance of ~ 1.26 Å (See Fig. S4B).

Thus, we can conclude, that the $S_1^{LE}(\pi,\pi^*)$ will structurally evolve to populate equilibrium of the $S_1(\pi,\pi^*)$ state. In its proximity is located a convenient crossing point $S_1(\pi,\pi^*)/S_1^{LU}(n,\pi^*)$ (Fig. 7A). The path $S_1(\pi,\pi^*) \rightarrow S_1^{LU}(n,\pi^*)$ is supported by close energy curve calculated $S_1^{LU}(n,\pi^*)$ for geometry of $S_1(\pi,\pi^*)$. This is not the case for the
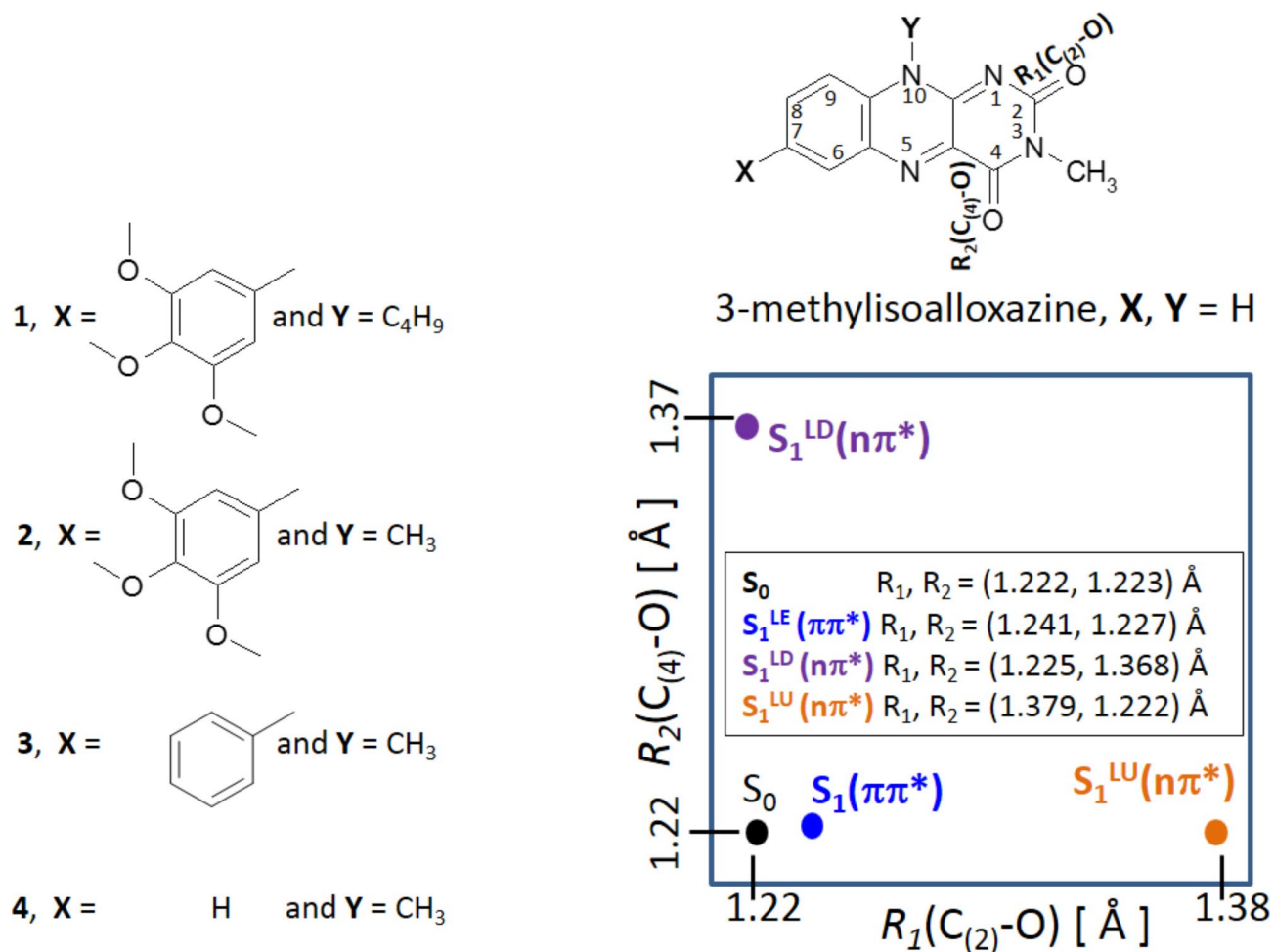
Fig. 6. Enumeration of atoms (right above) in the **Fl** derivatives (numbered **1–4**). In the rectangle (right below) shown is position of the ground, S_0, and three excited–state equilibrium forms: $S_1^{LE}(\pi,\pi^*)$, $S_1^{LD}(n,\pi^*)$, and $S_1^{LU}(n,\pi^*)$ for **1**, in the $[R_1, R_2]$ configuration space. Molecule **1** is 10-butyl-3-methyl-7-(3,4,5-trimethoxyphenyl)isoalloxazine, molecule **2** is 3,10-dimethyl-7-(3,4,5-trimethoxyphenyl)isoalloxazine, molecule **3** is 3,10-dimethyl-7-phenylisoalloxazine, molecule **4** is 3,10-dimethylisoalloxazine.
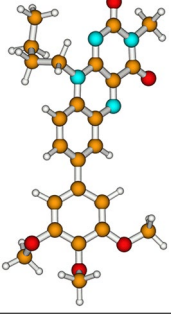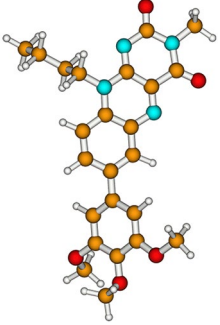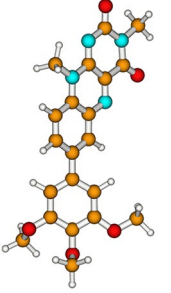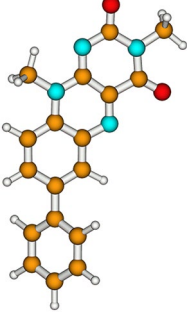
Probe wavelength [nm]	A_1	τ_1[ps]	A_2	τ_2[ps]	Offset
1513	0.0536	0.47	–	–	0.000022
1018	− 0.023	0.46	0.022	2.1	0.000023
650	− 0.020	0.62	0.010	2.2	− 0.000083
541	− 0.026	0.41	0.038	3.0	0.0000056
473	0.021	0.66	− 0.0087	3.4	− 0.00012

Table 1. Results of the fit of selected kinetic traces with single or double exponential function ($\Delta A = A_1 \exp\left(-\frac{t}{\tau_1}\right) + A_2 \exp\left(-\frac{t}{\tau_2}\right) + offset$) convoluted with instrument response function (ca. 200 fs, FWHM). Accuracy of time constants is ca. ± 10%.

alternative path $S_1(\pi,\pi^*) \rightarrow S_1^{LD}(n,\pi^*)$, since the $S_1^{LD}(n,\pi^*)$ state calculated on top of the profile $S_1^{LE}(\pi,\pi^*)$ lands over 1 eV higher in energy (Fig. S4) that allows us to exclude it from the $S_1(\pi,\pi^*)$ depopulation mechanism.

We propose that $S_1(\pi,\pi^*)/S_1^{LU}(n,\pi^*)$ conical intersection is responsible for short $S_1(\pi,\pi^*)$ state lifetime observed in the experiment (0.5 ps). Formed species in the $S_1^{LU}(n,\pi^*)$ state shows up evolution of the geometry of the molecule **1** due to the elongation of the $C_{(2)}$-O bond up to 1.38 Å (red curve, Fig. 7A). As the molecule relaxes in the $S_1^{LU}(n,\pi^*)$ state toward its minimum, internal conversion $S_1^{LU}(n,\pi^*) \rightarrow S_0$ becomes more probable since the respective energy difference $\Delta E(S_1^{LU}(n,\pi^*), S_0)$ gets smaller down to ~ 0.4 eV for the given equilibrium geometry of the $S_1^{LU}(n,\pi^*)$ state (Fig. 7A). Such a behavior of the $^1n\pi^*$ excited state related to the $C_{(2)}$-O bond

S_0 form			ΔE^{VE}[eV]	λ_{abs}[nm]	f	μ_e[D]
Molecule 1, H-bonded isomer						
S_0		S_0	0.00[a]			μ_g=6.5
		$S_0 \rightarrow S_1(\pi,\pi^*)$	2.76	450	0.2071	10.1
		$S_0 \rightarrow S_2(n,\pi^*)$	3.38	367	0.0010	1.6
		$S_0 \rightarrow S_3(n,\pi^*)$	3.45	360	0.0013	3.1
		$S_0 \rightarrow S_4(\pi,\pi^*)$	3.77	329	0.0146	21.9
		$S_0 \rightarrow S_5(\pi,\pi^*)$	4.00	310	0.0432	1.7
		$S_0 \rightarrow S_6(\pi,\pi^*)$	4.06	306	0.0269	21.6
Molecule 1, non-H-bonded isomer						
S_0		S_0	0.026[a]			μ_g=7.0
		$S_0 \rightarrow S_1(\pi,\pi^*)$	2.89	429	0.2308	9.3
		$S_0 \rightarrow S_2(n,\pi^*)$	3.37	368	0.0007	3.4
		$S_0 \rightarrow S_3(n,\pi^*)$	3.53	352	0.0012	3.7
		$S_0 \rightarrow S_4(\pi,\pi^*)$	3.94	315	0.0104	19.3
		$S_0 \rightarrow S_5(\pi,\pi^*)$	4.05	306	0.0380	1.6
		$S_0 \rightarrow S_6(n,\pi^*)$	4.16	298	0.0004	3.9
Molecule 2						
S_0		S_0	0.0[a]			μ_g=7.2
		$S_0 \rightarrow S_1(\pi,\pi^*)$	2.77	448	0.2305	10.5
		$S_0 \rightarrow S_2(n,\pi^*)$	3.30	376	0.0003	3.2
		$S_0 \rightarrow S_3(n,\pi^*)$	3.46	359	0.0006	3.8
		$S_0 \rightarrow S_4(\pi,\pi^*)$	3.75	331	0.0151	22.1
		$S_0 \rightarrow S_5(\pi,\pi^*)$	3.94	315	0.0583	1.8
		$S_0 \rightarrow S_6(\pi,\pi^*)$	4.06	306	0.0371	20.2
Molecule 3						
S_0		S_0	0.0[a]			μ_g=8.3
		$S_0 \rightarrow S_1(\pi,\pi^*)$	2.83	439	0.2298	9.6
		$S_0 \rightarrow S_2(n,\pi^*)$	3.30	376	0.0003	2.3
		$S_0 \rightarrow S_3(n,\pi^*)$	3.46	359	0.0006	4.7
		$S_0 \rightarrow S_4(\pi,\pi^*)$	3.93	316	0.0390	2.7
		$S_0 \rightarrow S_5(\pi,\pi^*)$	4.05	306	0.0855	13.3
		$S_0 \rightarrow S_6(n,\pi^*)$	4.08	304	0.0001	3.9
Molecule 4						
Continued						
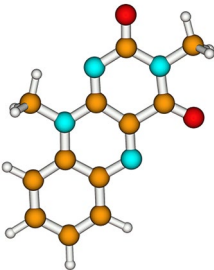
S_0 form		ΔE^{VE}[eV]	λ_{abs}[nm]	f	μ_e[D]
S_0	S_0	0.0			μ_g=7.9
	$S_0 \rightarrow S_1(\pi,\pi^*)$	3.01	412	0.2138	7.9
	$S_0 \rightarrow S_2(n,\pi^*)$	3.39	366	0.0004	1.5
	$S_0 \rightarrow S_3(n,\pi^*)$	3.51	354	0.0005	4.4
	$S_0 \rightarrow S_4(\pi,\pi^*)$	4.02	309	0.0955	2.9
	$S_0 \rightarrow S_5(n,\pi^*)$	4.19	296	0.0000	4.7
	$S_0 \rightarrow S_6(\pi,\pi^*)$	4.22	294	0.0723	11.4

Table 2. Absorption spectra of the studied molecules calculated with the CC2/aug-cc-pVDZ method at the geometry optimized at the MP2/cc-pVDZ theory level.

elongation as an important driving coordinate toward the conical intersection region has been reported for thymine[46]. Consequently, one can expect a short excited–state lifetime $\tau_{S1(n,\pi^*)}$ determined for molecule **1**. The nascent molecule in the S_0-state undergoes relaxation by shortening the $C_{(2)}$-O bond, thereby recovering the initial structure and completing the photocycle.

Observing the changes in a series of the excited-state profiles for molecules **4**, **3**, **2** and **1** (Figure S3) one can notice that the $S_1^{LD}(n,\pi^*)$ and $S_1^{LE}(\pi,\pi^*)$ excited states become more proximal to each other in terms of energy what makes the $S_1^{LE}(\pi,\pi^*)$ state depopulation faster in **1**. For instance, in the molecule **4** pattern of the excited-states energy profiles are less convenient for the deactivation, since equilibrium of the $S_1(\pi,\pi^*)$ state is more stable. The crossing point $S_1(\pi,\pi^*)/S_1^{LU}(n,\pi^*)$ is substantially less convenient to reach for **4** in comparison to **1**. The energy barrier is about 0.06 eV, at the $C_{(2)}$-O distance of ~ 1.29 Å for **4** (extended by 0.05 Å from its minimum) and the $S_1(\pi,\pi^*)$ state profile is monotonously increasing its energy towards longer $C_{(2)}$-O distances (Fig. S5). In **4** the access to the CI($^1\pi\pi^*/^1n\pi^*$) point is more difficult, which rationalizes the experimental data showing a long $S_1(\pi,\pi^*)$ excited-state lifetime (7 ns)[16].

We should emphasize that calculations are performed in the gas phase, while time-resolved experiments were performed in polar solvent as acetonitrile (compound **1** is not soluble in nonpolar solvent as *n*-hexane). One can expect that the selection of polar solvent influences the course of the potential-energy profiles of polar intermediates (see dipole moments in Table 3). Thus a direct comparison between the gas-phase calculation and experimental data recorded in the polar solvent is not straightforward. On the other hand, the calculations develop the mechanistic picture for $^1(\pi,\pi^*) \rightarrow ^1(n,\pi^*)$ path explaining a very fast $^1(\pi,\pi^*)$ deactivation in **1**.

The butyl group in molecule **1**, as a weak electron-donor, has a weak influence on energy potential profiles (Figure S3) upon comparison of molecule **1** (with butyl group) and molecule **2** (with methyl group) at position $N_{(10)}$. Thus, the presence of trimethoxyphenyl substituent is a key factor influencing the unique photophysics
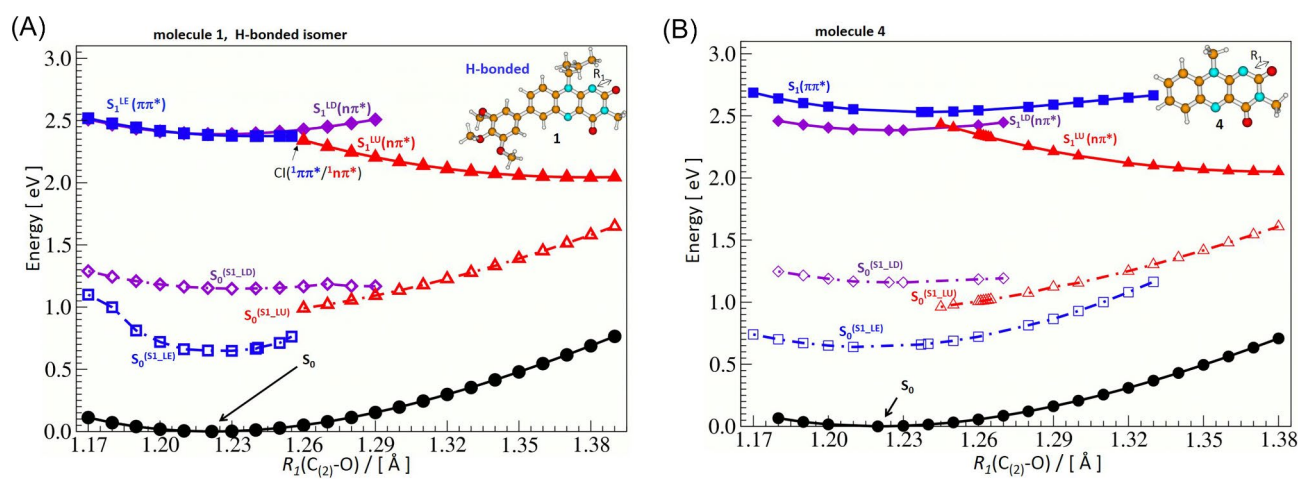

Fig. 7. Excited-state (S_1) potential-energy profile of **1** (**A**) and **4** (**B**) (calculated with the ADC(2)/cc-pVDZ method) plotted as a function of the $R_1(C_{(2)}$-O) distance to describe the S_1-state deactivation process through a cascade of the S_1 states leading toward the region with a low S_0-S_1 state energy gap. Solid lines and full symbols denote the ground (S_0), and excited S_1-state minimum energy profiles. Dashed lines and open symbols (S_0^{S1}) denote energy profiles of the ground S_0 state calculated at the optimized geometry of the given S_1 state. Black circles indicate the S_0 state, blue squares - $S_1(\pi,\pi^*)$, violet diamonds- $S_1^{LD}(n,\pi^*)$, and red triangles - $S_1^{LU}(n,\pi^*)$.

State	$S_1^{LE}(\pi,\pi^\star)$	$S_1^{LD}(n,\pi^\star)$	$S_1^{LU}(n,\pi^\star)$	S_0
Molecule 1, roatmer H-bonded				
E^a (S_1)	2.374 eV	2.389 eV	2.043 eV	0.00
$E_{fl.}$	1.71 eV (1.90 eV)	1.24 eV	0.47 eV	–
$f_{fl.}$	0.1112	0.0000007	0.000004	–
μ_e	6.0 D	4.3 D	10.3 D	6.5 D
R_1($C_{(2)}$-O)	1.241 Å	1.225 Å	1.379 Å	1.222 Å
R_2($C_{(4)}$-O)	1.227 Å	1.368 Å	1.222 Å	1.223 Å
R_3($C_{(4')}$H—$N_{(1)}$)	2.488 Å	2.502 Å	2.558 Å	2.487 Å
Molecule 1, rotamer non-H-bonded				
E^a (S_1)	2.465	2.441	2.074	0.026 eV
$E_{fl.}$	1.93 eV (2.09 eV)	1.27 eV	0.46 eV	–
$f_{fl.}$	0.1581	0.000003	0.000004	–
μ_e	7.4 D	4.0 D	10.5 D	6.7 D
R_1($C_{(2)}$-O)	1.234 Å	1.226 Å	1.379 Å	1.221 Å
R_2($C_{(4)}$-O)	1.229 Å	1.367 Å	1.222 Å	1.223 Å
R_3($C_{(4')}$H—$N_{(1)}$)	5.264 Å	5.243 Å	5.266 Å	5.159 Å
Molecule 2				
E^a (S_1)	2.443 eV	2.376 eV	2.028 eV	0.0 eV
$E_{fl.}$	1.98 eV	1.22 eV	0.43 eV	–
$f_{fl.}$	0.1801	0.0000006	0.000003	–
μ_e	7.9 D	4.3 D	10.2 D	6.8 D
R_1($C_{(2)}$-O)	1.234 Å	1.220 Å	1.380 Å	1.221
R_2($C_{(4)}$-O)	1.229 Å	1.368 Å	1.222 Å	1.223
Molecule 3				
E^a (S_1)	2.474 eV	2.378 eV	2.038 eV	0.0 eV
$E_{fl.}$	1.93 eV	1.22 eV	0.433 eV	–
$f_{fl.}$	0.1679	0.0000006	0.00003	–
μ_e	7.8 D	3.4 D	9.6 D	6.6 D
R_1($C_{(2)}$-O)	1.235 Å	1.224 Å	1.379 Å	1.220 Å
R_2($C_{(4)}$-O)	1.228 Å	1.368 Å	1.222 Å	1.223 Å
Molecule 4				
E^a (S_1)	2.531 eV	2.384 eV	2.051 eV	0.00
$E_{fl.}$	1.87 eV	1.22 eV	0.44 eV	–
$f_{fl.}$	0.1342	0.0000006	0.000003	–
μ_e	8.9 D	3.2 D	10.0 D	7.6 D
R_1($C_{(2)}$-O)	1.237 Å	1.224 Å	1.380 Å	1.220 Å
R_2($C_{(4)}$-O)	1.228 Å	1.368 Å	1.222 Å	1.223 Å

Table 3. Adiabatic energies, E^a (S_1) (in eV), fluorescence energy, $E_{fl.}$ (in eV), oscillator strength, f, dipole moment, μ_e, and carbonyl bond distances of the $S_1^{LE}(\pi,\pi*)$, $S_1^{LD}(n,\pi^\star)$ and $S_1^{LU}(n,\pi^\star)$ excited–state forms for three flavin derivatives optimized at the ADC(2)/cc-pVDZ theory level. Single point calculation of E_{fl} at the CC2/aug-cc-pVDZ level are given in parenthesis
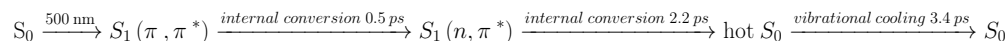
of molecule **1.** This conclusion corresponds to experimental values as other similar 10-butylisoalloxazines are characterized by usual "flavin" fluorescence parameters[19]

Conclusions

According to theoretical predictions for molecule **1**, the presence of a trimethoxyphenyl group in flavin opens the $^1(\pi,\pi^\star) \rightarrow {}^1(n,\pi^\star)$ deactivation channel. The electron donating group present in the studied molecules levels off the fluorescent $^1(\pi,\pi^\star)$ state relative to the dark $^1(n,\pi^\star)$ state, making S_1-state depopulation easier. The change in geometry occurring in the $^1(n,\pi^\star)$ state is related to the stretching of one of the C=O carbonyl bonds present in the isoalloxazine moiety. Consequently, there is a substantial decrease in the $S_1(n,\pi^\star)$-S_0 state energy gap, making the internal conversion channel effective and responsible for $^1(n,\pi^\star)$ excited-state depopulation to the S_0 ground state. This deactivation mechanism is unique and complements rare fast deactivation processes among flavin derivatives, e.g. "butterfly" bending motion described for partially or fully reduced isoalloxazine derivatives[47].

The effective internal conversion $^1(\pi,\pi^\star) \rightarrow {}^1(n,\pi^\star)$ explains the experimental data obtained for molecule **1**: a substantial shortening in the measured excited-state lifetimes (on the order of picoseconds for molecule **1**) compared to unsubstituted flavins as 3,10-dimethylisoalloxazine **4** (on the order of nanoseconds) as well as other

7-aryl-10-butylisoalloxazines[15]. The laser-pulse induced photoprocess in molecule **1** occurs within a 15 ps time window in acetonitrile. The mechanism $^1(\pi,\pi^*) \rightarrow {}^1(n,\pi^*) \rightarrow S_0$ is experimentally confirmed as the photoexcited $^1(\pi,\pi^*)$ state population decays mainly through the $^1(n,\pi^*)$ excited state intermediate, followed by recovery to the S_0 ground state. The absence of triplet excited state in the mechanism is also confirmed by the transient absorption spectroscopy. The emerging photoprocess is described by:

$$S_0 \xrightarrow{500\,nm} S_1(\pi,\pi^*) \xrightarrow{internal\ conversion\ 0.5\,ps} S_1(n,\pi^*) \xrightarrow{internal\ conversion\ 2.2\,ps} hot\ S_0 \xrightarrow{vibrational\ cooling\ 3.4\,ps} S_0$$

with a minor contribution of fluorescence (yield $\Phi_f = 2.6 \times 10^{-4}$). It should be mentioned that a significant weakening of fluorescence was also observed by the introduction of the 3,4,5-trimethoxyphenyl group into position 7 for 1,3-dimethylalloxazine and 5-phenyl-3,10-dimethyl-5-deazaisoalloxazine.[15] Unique properties of these derivatives can be used in applications that require minimal side-reactions caused by the singlet oxygen ($^1O_2$) or for organocatalysis to avoid participation of an excited form of flavin at all.

Data availability
The datasets generated during the current study are available from the corresponding author on request.

References

1. Massey, V. The chemical and biological versatility of Riboflavin. *Biochem. Sos Trans.* **28**, 283–296. https://doi.org/10.1042/bst0280283 (2000).
2. Cibulka, R. & Fraaije, M. W. *Flavin-Based Catalysis: Principles and Applications* (Viley-VCH, 2021).
3. Silva, E. & Edwards, A. M. *Flavins: Photochemistry and Photobiology* (Royal Society of Chemistry, 2006).
4. Sideri, I. K., Voutyritsa, E. & Kokotos, C. G. Photoorganocatalysis, small organic molecules and light in the service of organic synthesis: the awakening of a sleeping giant. *Org. Biomol. Chem.* **16**, 4596–4614. https://doi.org/10.1039/c8ob00725j (2018).
5. Romero, N. A. & Nicewicz, D. A. Organic photoredox catalysis. *Chem. Rev.* **116**, 10075–10166. https://doi.org/10.1021/acs.chemrev.6b00057 (2016).
6. Srivastava, V., Singh, P. K. & Singh, P. P. Recent advances of visible-light photocatalysis in the functionalization of organic compounds. *J. Photochem. Photobiol. C Photochem. Rev.* **50**, 100488. https://doi.org/10.1016/j.jphotochemrev.2022.100488 (2022).
7. Rehpenn, A., Walter, A. & Storch, G. Molecular editing of flavins for catalysis. *Synthesis* **53**, 2583–2593. https://doi.org/10.1055/a-1458-2419 (2021).
8. Iida, H., Imada, Y. & Murahashi, S. I. Biomimetic flavin-catalysed reactions for organic synthesis. *Org. Biomol. Chem.* **13**, 7599–7613. https://doi.org/10.1039/c5ob00854a (2015).
9. Sikorska, E., Sikorski, M., Steer, R. P., Wilkinson, F. & Worrall, D. R. Efficiency of singlet oxygen generation by alloxazines and isoalloxazines. *J. Chem. Soc. Faraday Trans.* **94**, 2347–2353. https://doi.org/10.1039/A802340I (1998).
10. Sikorska, E., Khmelinskii, I. V., Koput, J. & Sikorski, M. Electronic structure of lumiflavin and its analoguesin their ground and excited states. *J. Mol. Struct. (Theochem.)* **676**, 155–160. https://doi.org/10.1016/j.theochem.2004.02.007 (2004).
11. Sikorska, E. et al. Spectroscopy and photophysics of lumiflavins and lumichromes. *J. Phys. Chem. A* **108**, 1501–1508. https://doi.org/10.1021/jp037048u (2004).
12. Heelis, P. F. The photophysical and photochemical properties of flavins (isoalloxazines). *Chem. Soc. Rev.* **11**, 15–39. https://doi.org/10.1039/CS9821100015 (1982).
13. Kowalczyk, M. et al. Spectroscopy and photophysics of flavin-related compounds: Isoalloxazines. *J. Mol. Struct. (Theochem.)* **756**, 47–54. https://doi.org/10.1016/j.theochem.2005.09.005 (2005).
14. Sikorska, E., Khmelinskii, I. V., Worrall, D. R., Koput, J. & Sikorski, M. Spectroscopy and photophysics of iso- and alloxazines: experimental and theoretical study. *J. Fluoresc.* **14**, 57–64. https://doi.org/10.1023/B:JOFL.0000014660.59105.31 (2004).
15. Čubiňák, M. et al. Tuning the photophysical properties of flavins by attaching an aryl moiety via direct C–C bond coupling. *J. Org. Chem.* **88**, 218–229. https://doi.org/10.1021/acs.joc.2c02168 (2023).
16. Visser, A. J. W. G. & Müller, F. Absorption and fluorescence studies on neutral and cationic isoalloxazines. *Helv. Chim. Acta* **62**, 593–608. https://doi.org/10.1002/hlca.19790620227 (1979).
17. Kar, R. K. & Miller, A. F. Understanding flavin electronic structure and spectra. *WIREs Comput. Mol. Sci.* **12**, e1541. https://doi.org/10.1021/acs.jpcb.1c07306 (2022).
18. Pakiari, A. H., Slarhaji, M., Abdollahi, T. & Safapour, M. The redox potential of flavin derivatives as a mediator in biosensors. *J. Mol. Model.* **27**, 96. https://doi.org/10.1007/s00894-020-04650-8 (2021).
19. Kar, R. K., Chansen, S., Mroginski, M. A. & Miller, A. F. Tuning the quantum chemical properties of flavins via modification at C8. *J. Phys. Chem. B* **125**, 12654–12669. https://doi.org/10.1021/acs.jpcb.1c07306 (2021).
20. Etz, B. D., DuClos, J. M. & Vyas, S. Investigating the photochemistry of C7 and C8 functionalized N(5)-ethyl-flavinium cation: a computational study. *J. Phys. Chem. A* **124**, 4193–4201. https://doi.org/10.1021/acs.jpca.0c01938 (2020).
21. Salzmann, S. & Marian, C. M. The photophysics of alloxazine: a quantum chemical investigation in vacuum and solution. *Photochem. Photobiol. Sci.* **8**, 1655–1666. https://doi.org/10.1039/b9pp00022d (2009).
22. Chang, X.-P., Xie, X.-Y., Lin, S.-Y. & Cui, G. QM/MM study on mechanistic photophysics of alloxazine chromophore in aqueous solution. *J. Phys. Chem. A* **120**, 6129–6136. https://doi.org/10.1021/acs.jpca.6b02669 (2016).
23. Kabir, M. P., Ghosh, P. & Gozem, S. Electronic structure methods for simulating flavin's spectroscopy and photophysics: comparison of multi-reference, TD-DFT, and single-reference wave function methods. *J. Phys. Chem. B.* **128**, 7545–7557. https://doi.org/10.1021/acs.jpcb.4c03748 (2024).
24. Tolba, A. H., Vávra, F., Chudoba, J. & Cibulka, R. Tuning flavin-based photocatalytic systems for application in the mild chemoselective aerobic oxidation of benzylic substrates. *Eur. J. Org. Chem.* **10**, 1579–1585. https://doi.org/10.1002/ejoc.201901628 (2020).
25. Pokluda, A. et al. Robust photocatalytic method using ethylene-bridged flavinium salts for the aerobic oxidation of unactivated benzylic substrates. *Adv. Synth. Catal.* **363**, 1–10. https://doi.org/10.1002/adsc.202100024 (2021).
26. Pavlovska, T. et al. Primary and secondary amines by flavin-photocatalyzed consecutive desulfonylation and dealkylation of sulfonamides. *Adv. Synth. Catal.* **365**, 4662–4671 (2023).
27. McBride, R. A., Barnard, D. T., Jacoby-Morris, K., Harun-Or-Rashid, M. & Stanley, R. J. Reduced flavin in aqueous solution is nonfluorescent. *Biochemistry* **62**, 759–769. https://doi.org/10.1021/acs.biochem.2c00538 (2023).
28. Imada, Y., Iida, H., Ono, S., Masui, Y. & Murahashi, S. I. Flavin-catalyzed oxidation of amines and sulfides with molecular oxygen: biomimetic green oxidation. *Chem. Asian J.* **1**, 136–147. https://doi.org/10.1002/asia.200600080 (2006).

29. Golczak, A. et al. Tetramethylalloxazines as efficient singlet oxygen photosensitizers and potential redox–sensitive agents. *Sci. Rep.* **13**, 13426. https://doi.org/10.1038/s41598-023-40536-4 (2023).
30. LMFIT. *Non-Linear Least-Square Minimization and Curve-Fitting for Python (0.8.0)* (Zenodo, 2014).
31. Wendel, M. et al. Time-resolved spectroscopy of the singlet excited state of betanin in aqueous and alcoholic solutions. *Phys. Chem. Chem. Phys.* **17**, 18152–18158. https://doi.org/10.1039/c5cp00684h (2015).
32. Gierczyk, B., Murphree, S. S., Rode, M. F. & Burdzinski, G. Blockade of persistent colored isomer formation in photochromic 3*H*–naphthopyrans by excited–state intramolecular proton transfer. *Sci. Rep.* **12**, 19159. https://doi.org/10.1038/s41598-022-23759-9 (2022).
33. Møller, C. & Plesset, M. S. Note on an aproximation treatment for many-electron systems. *Phys. Rev.* **46**, 618–622. https://doi.org/10.1103/PhysRev.46.618 (1934).
34. Hättig, C. *Advances in Quantum Chemistry* (ed Jensen, H. J. Å.), Vol. 50, 37–60 (Academic Press, 2005).
35. Schirmer, J. Beyond the random-phase approximation: a new approximation scheme for the polarization propagator. *Phys. Rev. A* **26**, 2395–2416. https://doi.org/10.1103/PhysRevA.26.2395 (1982).
36. Trofimov, A. B. & Schirmer, J. An efficient polarization propagator approach to valence electron excitation spectra. *J. Phys. B Mol. Opt. Phys.* **28**, 2299–2324. https://doi.org/10.1088/0953-4075/28/12/003 (1995).
37. Tuna, D. et al. Assessment of approximate coupled-cluster and algebraic-diagrammatic-construction methods for ground- and excited-state reaction paths and the conical-intersection seam of a retinal-chromophore model. *J. Chem. Theory Comput.* **11**, 5758–5781. https://doi.org/10.1021/acs.jctc.5b00022 (2015).
38. Dunning, T. H. Jr. Gaussian basis sets for use in correlated molecular calculations. I. The atoms boron through neon and hydrogen. *J. Chem. Phys.* **90**, 1007–1023. https://doi.org/10.1063/1.456153 (1989).
39. Christiansen, O., Koch, H. & Jørgensen, P. The second-order approximate coupled cluster singles and doubles model CC2. *Chem. Phys. Lett.* **243**, 409–418. https://doi.org/10.1016/0009-2614(95)00841-Q (1995).
40. Hättig, C. & Weigend, F. CC2 excitation energy calculations on large molecules using the resolution of the identity approximation. *J. Chem. Phys.* **113**, 5154–5161. https://doi.org/10.1063/1.1290013 (2000).
41. *TURBOMOLE V7.1 2016, a Development of University of Karlsruhe and Forschungszentrum Karlsruhe GmbH, 1989–2007, TURBOMOLE GmbH.* http://www.turbomole.com (2016).
42. Mojr, V. et al. Flavin photocatalysts for visible-light [2+ 2] cycloadditions: structure, reactivity and reaction mechanism. *CheCatChem* **10**, 1–11. https://doi.org/10.1002/cctc.201701490 (2018).
43. Oziminski, W. P. & Dobrowolski, J. C. s- and p-electron contributions to the substituent effect: natural population analysis. *J. Phys. Org. Chem.* **22**, 769–778. https://doi.org/10.1002/poc.1530 (2009).
44. Dobrowolski, J. C., Lipinski, P. F. J. & Karpinska, G. Substituent effect in the first excited singlet state of monosubstituted benzenes. *J. Phys. Chem. A* **122**, 4609–4621. https://doi.org/10.1021/acs.jpca.8b02209 (2018).
45. Rode, M. F. & Sobolewski, A. L. Effect of chemical substituents on energetical landscape of a molecular switch: an ab initio study. *J. Phys. Chem. A* **114**, 11879–11889. https://doi.org/10.1021/jp105710n (2010).
46. Perun, S., Sobolewski, A. L. & Domcke, W. Conical intersections in thymine. *J. Phys. Chem. A* **110**, 13238–13244. https://doi.org/10.1021/jp0633897 (2006).
47. Kao, Y. T. et al. Ultrafast dynamics of flavins in five redox states. *J. Am. Chem. Soc.* **130**, 7695–7701. https://doi.org/10.1021/ja8045469 (2008).

Acknowledgements

Author contributions

S. N.: data aquisition, apparatus construction, writing the manuscript & editing, N. V.: data aquisition, M. S. conceptualization, writing the manuscript & editing, T. T. : synthesis, E. S. : synthesis, R. C.: conceptualization, synthesis, writing the manuscript & editing, M. R.: calculations, conceptualization, visualization, writing the manuscript & editing, G. B.: data aquisition, formal analysis, conceptualization, visualization, writing the manuscript & editing All authors reviewed the manuscript.

Declarations

Competing interests

The authors declare no competing interests.

Additional information

Supplementary Information The online version contains supplementary material available at https://doi.org/10.1038/s41598-024-75239-x.

Correspondence and requests for materials should be addressed to M.S., R.C., M.F.R. or G.B.

Reprints and permissions information is available at www.nature.com/reprints.

Publisher's note Springer Nature remains neutral with regard to jurisdictional claims in published maps and institutional affiliations.